Highly Efficient, Color-Pure, Color-Stable Blue Quantum Dot Light-Emitting Devices

Ki-Heon Lee,[†] Jeong-Hoon Lee,[†] Woo-Seuk Song,[†] Heejoo Ko,[‡] Changho Lee,[‡] Jong-Hyuk Lee,[‡] and Heesun Yang[†,*]

[†]Department of Materials Science and Engineering, Hongik University, Seoul 121-791, Korea and [‡]Display Research Center Samsung Display Company, Ltd., Yongin, Kyunggi-do 446-811, Korea

ABSTRACT For colloidal quantum dot light-emitting diodes (QD-LEDs), blue emissive device has always been inferior to green and red counterparts with respect to device efficiency, primarily because blue QDs possess inherently unfavorable energy levels relative to green and red ones, rendering hole injection to blue QDs from neighboring hole transport layer (HTL) inefficient. Herein, unprecedented synthesis of blue CdZnS/ZnS core/shell QDs that exhibit an exceptional photoluminescence (PL) quantum yield of 98%, extraordinarily large size of 11.5 nm with a shell thickness of 2.6 nm, and high stability against a repeated purification process is reported. All-solution-processed, multilayered blue QD-LEDs, consisting of an HTL of poly(9-vinylcarbazole), emissive layer of CdZnS/ZnS QDs, and electron transport layer of ZnO nanoparticles, are fabricated. Our best device displays not only a maximum luminance of 2624 cd/m^2, luminous efficiency of 2.2 cd/A, and external quantum efficiency of 7.1%, but also no red-shift and broadening in electroluminescence (EL) spectra with increasing voltage as well as a spectral match between PL and EL.

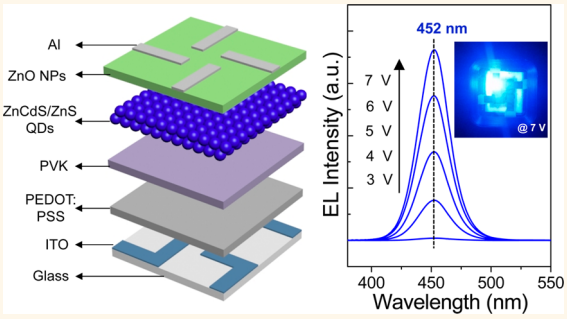

KEYWORDS: blue quantum dot · light-emitting diode · high-efficiency · high-color stability

Since the first introduction of semiconducting quantum dots (QDs) as an active emissive layer (EML) for light-emitting diode (LED) fabrication in 1994,[1] the steady improvements in device performance of QD-based LED (QD-LED) have been made, primarily through diversifying the type and deposition processing of constituent layers of device as well as refining the design and synthesis of core/shell QD structure. One of the prerequisites for realizing highly efficient, bright QD-LED is to utilize the QDs with high photoluminescence (PL) quantum yield (QY). Originally high QY of conventional core/shell QDs becomes substantially reduced after the repeated cycle of QD purification and/or the integration processing to solid-state QD film due to the physical separation of organic ligands from QD surface.[2−6] Therefore, more robust QDs that are not susceptible to the above subsequent processes and thus retain the original QY have been demonstrated in the form of multishell QD[4,5] (*e.g.*, core/gradient-composition shell/outer shell) or giant shell QD.[6] To maximize the electrically driven QD emission from QD-LED, the choice of charge transport layers (CTLs) on the basis of their energetic positions of highest occupied molecular orbital (HOMO) and lowest unoccupied molecular orbital (LUMO) relative to QDs is of great importance to facilitate charge carrier injection from anode/cathode and balance the injected carriers. Although various vacuum-deposited organic small molecules such as 2,2′,2″-(1,3,5-benzinetrily)tris(1-phenyl-1-*H*-benzimidazole) (TPBi)[3,7−11] and tris-(8-hydroxyquinoline)aluminum (Alq_3)[2] have been attempted previously as electron transport layers (ETLs) in QD-LEDs, recent researches revealed that inorganic ETLs of ZnO[12−15] and TiO_2[16,17] are much more advantageous, since they can be solution-processed, more stable against environmental moisture/oxygen, and more importantly, generate a desirable energy alignment between QD LUMO and ETL LUMO for efficient electron injection. In the case of hole transport layer (HTL), even though several organic or

* Address correspondence to hyang@hongik.ac.kr.

Received for review June 7, 2013 and accepted July 15, 2013.

Published online July 15, 2013
10.1021/nn402870e

inorganic HTLs such as poly(9-vinlycarbazole) (PVK),[12] poly[(9,9-dioctylfluorenyl-2,7-diyl)-*co*-(4,4′-(*N*-(4-*sec*-butylphenyl))diphenylamine)] (TFB),[16,17] and MoO_3[13,15] have been often adopted, the most common HTL to date is poly(*N*,*N*′-bis(4-butylphenyl)-*N*,*N*′-bis(phenyl)-benzidine) (poly-TPD).[2,9−11,14,18] This is because poly-TPD is quite resistant to typical solvents (*e.g.*, toluene, chloroform) where QDs are dispersed. Thus, the previously coated poly-TPD HTL can survive with a minimal damage after solution-processing of QD solution. Holloway *et al.* reported on the impressive device performance of QD-LEDs with all solution-processed hybrid CTLs, consisting of an HTL of poly-TPD, an ETL of ZnO nanoparticles (NPs), and EMLs of emission color-tuned CdSe/ZnS QDs, exhibiting peak luminances of 4200, 68 000, and 31 000 cd/m^2 and maximum external quantum efficiencies (EQEs) of 0.22, 1.8, and 1.7% from blue (470 nm), green (540 nm), orange-red (600 nm) emissive devices, respectively.[14] Later, Kwak *et al.* fabricated more bright, efficient QD-LEDs with an inverted structure, displaying even better device characteristics, *i.e.*, maximum EQEs of 1.7, 5.8, and 5.7% and maximum luminances up to 2250, 218 000, and 23 040 cd/m^2 from blue (437 nm), green (520 nm), and red (628 nm) QD-LEDs, respectively.[15] Furthermore, very recently, the exceptionally high EQE of 18%, which was estimated to be close to the theoretical maximum of 20%, was realized from a red (around 615 nm) QD-LED that was fabricated in an inverted device scheme with partially solution-processed hybrid CTLs.[19]

As recognized from the above values, the device performance of blue QD-LED is always lower those of green and red ones, mainly attributable to the following points. First, compared to HOMO levels of green and red QDs, blue QD inherently possesses a lower HOMO level and thus a larger potential energy barrier at QD/HTL interface, rendering hole injection from neighboring HTL into QD more difficult and ultimately, leading to a poor EQE. Second, the photometric quantity of luminance, which is determined by the relative sensitivity of human vision to different wavelengths, shows a much lower luminous efficacy for blue light *versus* green and red counterparts. As a consequence of these two combined factors, low levels of luminance and luminous efficiency (LE, cd/A) naturally result from blue emissive device. The highest EQE and LE reported to date from state-of-the-art blue QD-LEDs did not exceed 2% and 0.5 cd/A, respectively. Herein, highly fluorescent blue (452 nm) alloyed QDs of CdZnS core/ZnS shell are first synthesized, and a surprisingly high PL QY of near-unity is for the first time realized by optimizing the ZnS shelling time. Intriguingly, the average sizes of the present CdZnS/ZnS QDs are larger than those of QDs reported in the literature. For the fabrication of all-solution-processed blue QD-LEDs, ZnO NPs and PVK, that is, a much cheaper than widely used poly-TPD, are utilized for the formation of ETL and HTL, respectively. From the viewpoint of processing compatibility, hexane is chosen for dispersing QDs, because it does not dissolve PVK. Consequently, previously deposited PVK HTL remains undamaged after spin-coating of QD solution in hexane. Our all-solution-processed blue QD-LED exhibits the record values of maximum LE of 2.2 cd/A and EQE of 7.1%. Moreover, unusual spectral match between PL and electroluminescence (EL) and no red-shift and broadening in EL spectra with increasing voltage are also reported.

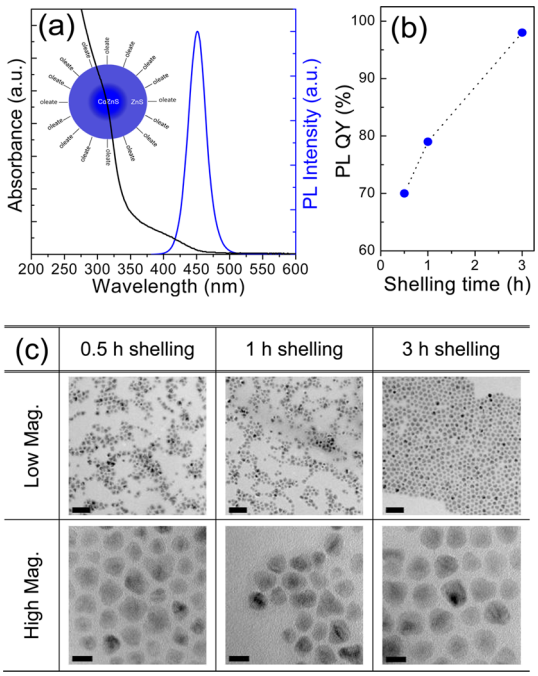

Figure 1. (a) Absorption and PL emission spectra of 3 h-shelled CdZnS/ZnS QDs (inset: a schematic of blue QDs with CdZnS/ZnS core/shell structure and oleate capping ligand). (b) Variation of PL QY and (c) low- (scale bar, 50 nm) and high-magnification (scale bar, 10 nm) TEM images of CdZnS/ZnS QDs with different shelling times of 0.5, 1, and 3 h.

RESULTS AND DISCUSSION

CdZnS/ZnS QDs have been synthesized with substantial modifications from the protocol in the literature.[20] To a mixture of CdO and Zn(acet)$_2$ in oleic acid (OA) was injected S solution in octadecene (ODE) at 310 °C, and the reaction was maintained for 12 min at that temperature. For ZnS shell overcoating, S-OA stock solution instead of conventional *S*-trioctylphosphine (S-TOP) or *S*-tributylphosphine (S-TBP) was consecutively introduced into the above CdZnS core QDs, and the shelling procedure lasted for up to 3 h at 310 °C. It should be noted that this shelling duration is extraordinarily long compared to those (*e.g.*, 10−40 min) adopted in the conventional shell overcoating. Typical CdZnS/ZnS QDs showed no surface-defect emission, purely consisting of a band edge emission with a peak wavelength of 452 nm and a bandwidth of 31 nm (Figure 1a). The peak wavelength

of blue emission could be also tailored finely in the range of 435−460 nm (approximately) simply by varying either the starting Cd/Zn precursor ratio or the amount of S-ODE solution. As seen from the shelling duration-dependent PL QY variation of Figure 1b, PL QY kept increasing from 70% for 0.5 h-shelled QDs to 98% for 3 h-shelled ones. This exceptional QY of a near-unity from 3 h-shelled QDs is the highest value for blue QDs reported to date, even though 95−100% QYs from green and red QDs were found in the recent literature.[4,5] A higher QY of 3 h-shelled QDs *versus* 0.5 h-shelled ones indicates that a more perfect surface passivation of CdZnS core QDs with ZnS shell could be afforded by a longer shelling duration, which might lead to the structural improvement at CdZnS/ZnS interface *via* the effective thermal annealing. More specifically, this sufficiently long shelling at a temperature of 310 °C, which is high enough to induce the interfacial alloying,[20] would render the core/shell boundary less abrupt, creating compositionally more or less smooth interface. Concomitantly, the emission wavelength of CdZnS/ZnS QDs became a bit blue-shifted with a longer shelling time (Figure S1a), *i.e.*, 456 nm for 0.5 h- *versus* 452 nm for 3 h-shelled QDs, indicative of slight alloying *via* Zn diffusion into core. It is also worth noting that all QY values in Figure 1b were recorded from the QDs obtained after 3 time-repeated purification cycle. While most QDs that exhibit a high initial QY very often suffer from a severe reduction in QY after the purification cycle, all of our CdZnS/ZnS QDs regardless of shelling duration were immune to such deterioration. The 3 h-shelled QDs were purified up to 3 times and the change of PL QY with the repetition number of purification was monitored. PL QY rather increased from 88 to 98% as the purification step was repeated, attributable to a gradual removal of byproducts and unreacted species. To validate the superiority of our OA-capped CdZnS/ZnS QDs with respect to the fluorescent stability against purification step, TOP-capped CdZnS/ZnS QDs with an average size of 8.5 nm (Figure S2a) were separately synthesized by applying S-TOP stock solution to the same CdZnS core QDs and maintaining the shelling reaction for 30 min. The resulting TOP-capped CdZnS/ZnS QDs exhibited a typical QY reduction, rapidly dropping from 74% from as-taken QDs to 38% from 3 time-purified ones (Figure S2b), due to the gradual detachment of TOP ligands from QD surface. Thus, these comparative results indirectly evidence that, compared to TOP, OA would be more strongly coordinated with S atom on QD surface, thereby preventing the loss of capping ligands during purification cycle. In addition, PL QY of about 20 nm-thick, solid-state QD films spin-deposited on bare glass substrate has been collected using an absolute PL QY measurement system (C9920-02, Hamamatsu) in an integrating sphere. The 0.5 h-, 1 h-, and 3 h-shelled CdZnS/ZnS QD films exhibited somewhat reduced QY values of 58, 67, and 86%, respectively, compared to the aforementioned results from dilute QD solution samples. PL spectra between solid-state QD film and dilute QD solution were also found to almost match without observing a noticeable peak shift, as compared in normalized PL spectra of the representative 3 h-shelled QDs (Figure S2c).

Low- and high-magnification transmission electron microscopic (TEM) images of CdZnS/ZnS QDs with different shelling durations are compared in Figure 1c. The 0.5 and 1 h-shelled QDs exhibited somewhat nonuniform shapes along with relatively broad size distributions and similar average sizes of ∼9.5 nm. Meanwhile, 3 h-shelling led to the marked improvements in shape uniformity and size distribution. Moreover, their size impressively increased up to 11.5 nm (corresponding to about 8.5 monolayers (MLs)) of ZnS, based on the average size (6.3 nm) of spherical CdZnS core QDs (Figure S3a). The change in actual Zn/Cd ratio of CdZnS/ZnS QDs with different shelling times, obtained by an energy dispersive spectroscopy (EDS) (Figure S1b), is also consistent with the above size increase as a result of the growth of a thicker shell, indicating that under our shelling strategy particularly using S-OA solution the shell continually grew during a relatively long shelling period without the introduction of an additional shell stock solution. Compared to the conventional QDs of core/shell structure that exhibit typical mean diameters < ∼8 nm regardless of their emission color, the sizes of our blue QDs were abnormally big (especially in the case of 3 h-shelled ones), even though the giant QDs with ultra-thick shells of >10 MLs in CdSe/CdS core/shell system are available in the literature.[6,21−25] PL QY of such giant QDs usually tends to decrease with increasing shell thickness due to the formation of higher defect density within a thicker shell,[6,25] which is contrast to our observation that 3 h-shelled QDs with a thicker shell showed a higher PL QY than 0.5 or 1 h-shelled ones with relatively thin shells.

Blue QD-LED was fabricated by sequentially spin-coating the solutions of poly(ethylenedioxythiophene): polystyrene sulfonate (PEDOT:PSS), PVK in chlorobenzene, CdZnS/ZnS QDs in hexane, and ZnO NPs in ethanol (Figure 2a). ZnO NPs were prepared by precipitation from $Zn(acet)_2$ and tetramethylammonium hydroxide (TMAH), exhibiting a size distribution of 3.0−3.5 nm as shown in TEM image of Figure S3b. A schematic of all-solution-processed blue QD-LED with a multilayered structure, consisting of a patterned indium tin oxide (ITO)/33 nm thick PEDOT:PSS/22 nm thick PVK/23 nm thick (3 h-shelled) CdZnS/ZnS QDs/30 nm thick ZnO NPs/Al, is shown in Figure 2b. A photograph of the completed device, consisting of 4 emitting spots with an area of 9 mm^2, is also presented in Figure 2c. Because of the insolubility of PVK in hexane, the predeposited PVK HTL was preserved perfectly

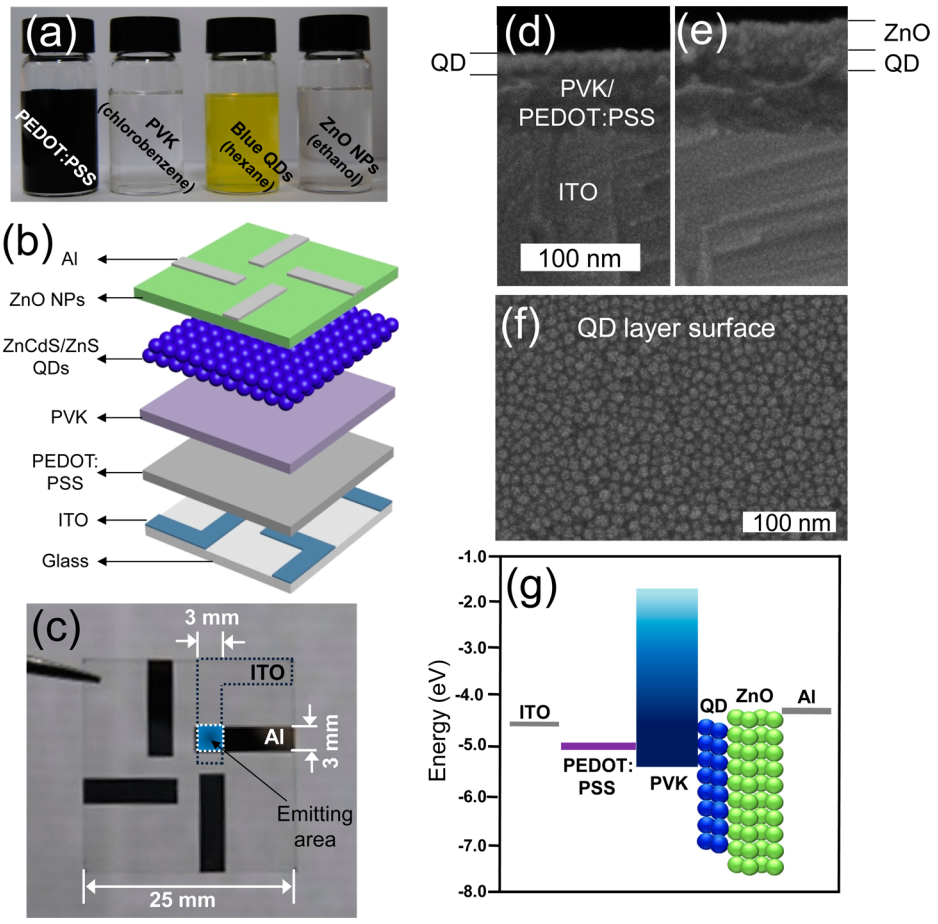

Figure 2. (a) Coating solutions of PEDOT:PSS, PVK in chlorobenzene, CdZnS/ZnS QDs in hexane, and ZnO NPs in ethanol. (b) Schematic illustration of all-solution-processed blue QD-LED with a multilayered structure, consisting of ITO/PEDOT:PSS/PVK/ CdZnS/ZnS QDs/ZnO NPs/Al. (c) Photograph of the completed device, consisting of 4 emitting spots with an area of 9 mm^2. Cross-sectional SEM images of ITO/PEDOT:PSS/PVK/QDs (d) without and (e) with ETL of ZnO NPs. (f) Surface SEM image of ITO/ PEDOT:PSS/PVK/QDs. (g) Energy levels of multilayered structure.

after the coating process of QD-hexane dispersion. Well-defined multilayered structure can be seen from the cross-sectional scanning electron microscopic (SEM) images of ITO/PEDOT:PSS/PVK/QDs without (Figure 2d) and with ETL of ZnO NPs (Figure 2e). The surface SEM image of ITO/PEDOT:PSS/PVK/QDs clearly shows that the spin-coated QD layer possesses the uniform surface morphology and consists of well orderly, packed QDs (Figure 2f). The spin-coated layer of ZnO NPs was also uniformly, smoothly formed on top of EML of QDs, as seen from Figure S4. Atomic force microscope (AFM) images of QD and ZnO NP layer surfaces having root-mean-square roughness values of 3.2 a nd 3.8 nm, respectively, are also shown in Figure S5. As expected from the schematic energy diagram of Figure 2g, ZnO NP layer having an electron affinity of ~4.3 eV and an ionization potential of ~7.6 eV[14] functions as an appropriate ETL for not only facilitating the injection of electrons to QDs, but also blocking a hole transport at QD/ETL interface and consequently providing the increased exciton recombination efficiency at QD region.

Figure 3a presents voltage-dependent variations of luminance and current density of 3 QD-LED devices having blue QDs with different shelling times. Note that in this work 6 sets of the above 3 devices were repeatedly fabricated, and the data below represent the mean values for each QD-LED. Under the same voltage of 7.5 V, maximum luminances of 1225, 1904, and 2624 cd/m^2 for 0.5, 1, and 3 h-shelled QD-based devices, respectively, were obtained. The increasing maximum luminance from 0.5, 1 to 3 h-shelled QD-based devices would be partly ascribed to a higher PL QY of the QDs with a longer shelling time (Figure 1b). The current densities of 0.5 h- and 1 h-shelled QD-LEDs were roughly similar, *e.g.*, 321 and 329 mA/cm^2 at an applied voltage of 7.5 V, respectively, but higher than that (*e.g.*, 234 mA/cm^2 at the same voltage) of 3 h-shelled one. Lower current densities observed from the latter device indicate that the charge injection might be more hindered by the presence of thicker shell as a nontrivial energetic barrier, resulting in the reduced bulk current. Together, the QD layer comprising bigger-sized QDs of 3 h shelling would be expected to not only be a bit thicker, but also contain a larger inter-QD void volume as compared with those from 0.5 and 1 h shelling QDs (assuming the same QD MLs of

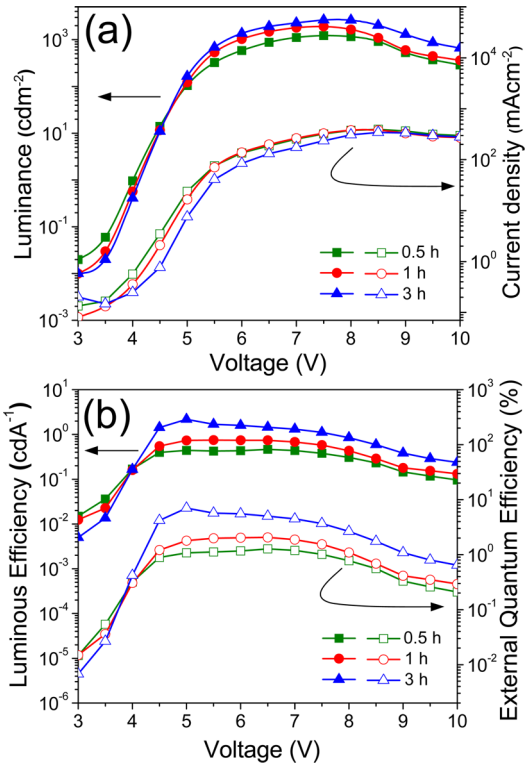

Figure 3. Voltage-dependent variations of (a) luminance and current density and (b) luminous efficiency and external quantum efficiency of 3 QD-LED devices based on blue QDs with different shelling times.

EML formed for all cases), limiting the current flow. Lower leakage currents together with higher luminances ultimately give rise to the substantially improved device efficiency from 3 h-shelled QD-LED relative to 0.5 and 1 h-shelled ones, as described below. Figure 3b depicts the characteristics of LE and EQE as a function of voltage. The peak LEs from 0.5, 1, and 3 h-shelled QD-based devices were 0.4, 0.7, and 2.2 cd/A, respectively, at a driving voltage of 5 V. While the peak LE of 0.5 h-shelled QD-LED was comparable to the best maximum LE values (0.32 cd/A for 470 nm-emitting QD-LED[14] and 0.4 cd/A for 437 nm-emitting one[15]) reported in the literature, 3 h-shelled QD-LED exhibited a much higher peak LE by more than 5 times compared to the above best values and a still high LE of about 1.6 cd/A even at a luminance level of 1000 cd/m^2 (Figure S6a). As seen in the characteristics of power efficiency (PE)-voltage (Figure S6b) from the same set of devices, the peak PEs were measured to be 0.3, 0.5, and 1.4 lm/W for 0.5, 1, and 3 h-shelled QD-LEDs, respectively. Since the LE and PE are sensitively dependent on the emission wavelength even in the same blue spectral window, the EQE value can be a better indicator for evaluating the device efficiency. The highest EQE value reported to date for blue QD-LEDs only reached 1.7% from the partially solution-processed device with an inverted structure.[15] As shown in Figure 3b, our 0.5, 1, and 3 h-shelled QD-LEDs displayed the peak EQEs of 1.1, 1.8, and 7.1%, respectively. In particular, an excellent EQE of 7.1% from 3 h-shelled QD-LED exceeds the efficiency from the above best device by more than 4 times. It is noted that the QDs with a little shorter (2.5 h) and even longer (4.5 h) shelling durations than 3 h were also synthesized and identically processed for QD-LED fabrication with the purpose of realizing an even higher-performance device through a further optimization of QD shelling; however, the results showed no meaningful difference among QD-LEDs having relatively long (*i.e.*, 2.5, 3, and 4.5 h)-shelled QDs, exhibiting overall the same device characteristics within an experimental error range. For a direct comparison, a control device based on TOP-capped CdZnS/ZnS QDs was also fabricated and exhibited a maximum luminance of 379 cd/m^2 at 8 V, LE of 0.3 cd/A, and EQE of 0.9% at 6 V at best (Figure S7).

Compared to the moderate increase in EQE of 1 h-shelled QD-LED *versus* 0.5 h-shelled one, the EQE increase of 3 h-shelled *versus* 1 h-shelled device is surprisingly substantial (specifically, showing an over 3-fold raise in peak EQE), which is attributable to the combined effect of several factors. First, a higher PL QY of 3 h-shelled QDs *versus* 1 h-shelled ones should definitely, but partly, lead to the improved device efficiency. Second, a larger size, *i.e.*, a thicker shell, of 3 h-shelled QDs *versus* 1 h-shelled ones is likely to be one of the key factors for EQE enhancement. The shell thicknesses of 1 and 3 h-shelled QDs were about 1.6 and 2.6 nm, respectively (Figure 1c). Compared to the typical shell thickness of $\leq$1 nm for the conventional QDs, 3 h-shelled QDs possess a considerably thick ZnS shell. Giant shell QDs, typically consisting of CdSe/CdS combination with the minimum lattice mismatch between core and shell materials, have been devised to suppress PL blinking,[6,21,24] which arises from QD charging process. The charged QDs are placed under a very efficient nonradiative Auger recombination (AR) process, where the energy of electron–hole pairs is transferred to extra charge carriers, finally quenching the fluorescence. It is well-known that AR efficiency decreases linearly with increasing QD volume or shell thickness.[21,24] If compared to the QD blinking situation, QD-LED is more susceptible to QD charging. Not only the difference in potential barriers for hole and electron injection to QDs (as expected from the schematic energy diagram of Figure 2g), but different conductivities of ETL and HTL cause an imbalanced carrier injection to QD region, resulting in a significant QD charging. The charged excitons readily lose their energy through AR process, substantially limiting the device efficiency. In this context, 3 h-shelled QDs with a thick shell would be more advantageous in suppressing AR and consequently increasing the device efficiency than 1 h-shelled ones with a thin shell. Third, in addition to the formation of ultra-thick shell, the

control of core/shell interface is also critical in effectively reducing AR process and thus blinking probability. Although AR is highly efficient in the QDs with the abrupt confinement potential at core/shell interface, smoothing an interfacial potential between core/shell can significantly suppress AR.[22,26,27] Smoothing of the confinement potential can be achieved by forming an alloyed interface at core/shell. Taking into account that a higher degree of interfacial alloying is expected with a longer shelling duration at a high temperature of 310 °C as discussed earlier, the core/shell interface of 3 h-shelled QDs would be more smooth and beneficial for AR suppression than that of 1 h-shelled ones. To sum up, a thicker shell and a more smooth core/shell interface of longer-shelling QDs *versus* short-shelling ones are strongly believed to play a crucial role in substantially decreasing AR probability for the improvement of the device efficiency. Lastly, undesired resonant dipole−dipole energy transfer between the neighboring QDs in the closely packed QD ensemble should be minimized for the realization of high-efficiency QD-LED.[25] The presence of thick shell as an effective physical barrier lowers the probability of nonradiative resonant energy transfer between interacting QD dipoles. In the case of the QD layer close-packed with 3 h-shelled QDs, the core surfaces of neighboring QDs is separated by at least ~5.2 nm (also, corresponding to ~11.5 nm in core center-to-core center distance), and the distance becomes even longer when surface organic ligands are considered. This spacing is distant sufficiently to effectively limit the inter-QD resonant energy transfer,[8] ultimately leading to a high-efficiency QD-LED.

Most of QD-LEDs reported in the literature exhibit a red-shift along with spectral broadening of EL *versus* PL due to the dielectric function of surrounding medium[28] and/or the energy transfer from smaller to large QDs in the ensemble.[2,3,7,9,10,15] Consistent with no red-shift in PL of solid-state QD film *versus* dilute QD solution (Figure S2c), however, EL of our 3 h-shelled QD-LED almost matches with respect to peak position (452 nm) and bandwidth (31 nm) with PL of the dilute QD solution (Figure 4a), indicative of the effective suppression of the energy transfer. EL spectra of conventional QD-LEDs are usually red-shifted with increasing voltage owing to the so-called quantum confined Stark effect (QCSE),[28] a phenomenon that under an electric field the valence and conduction bands are titled and the polarization of electron−hole pairs occurs, which lowers the energetic difference between electron and hole states, finally leading to a red-shift of emission energy.[29] Simultaneously, EL bandwidth becomes broader with a higher voltage, and this spectral broadening is attributable to a larger exciton polarization under a higher electric field, resulting in the increased LO (longitudinal optical)-phonon coupling.[28] However, as shown in Figure 4b, EL spectra of 3 h-shelled QD-LED peaked at the same wavelength of 452 nm, showing no QCSE, and their bandwidths remained unchanged, independent of applied voltage. A thick ZnS shell of 3 h-shelled QDs is likely to act as an effective physical barrier to screen the external fields, preventing the polarization of electron−hole pairs. The results in Figure 4a,b are in contrast to those from TOP-capped CdZnS/ZnS QD-based LED, which showed a typical red-shift of EL *versus* PL along with red-shift/broadening in EL spectra with increasing voltage (Figure S8). Naturally, the Commission Internationale de l'Eclairage (CIE) color coordinates corresponding to the blue emission spectra in Figure 4b were positioned in a deep pure blue territory with identical coordinates of (0.153, 0.027), as marked in Figure 4c. A photograph of highly bright, color-saturated 3 h-shelled QD-LED operated at 7 V is shown in Figure 4d.

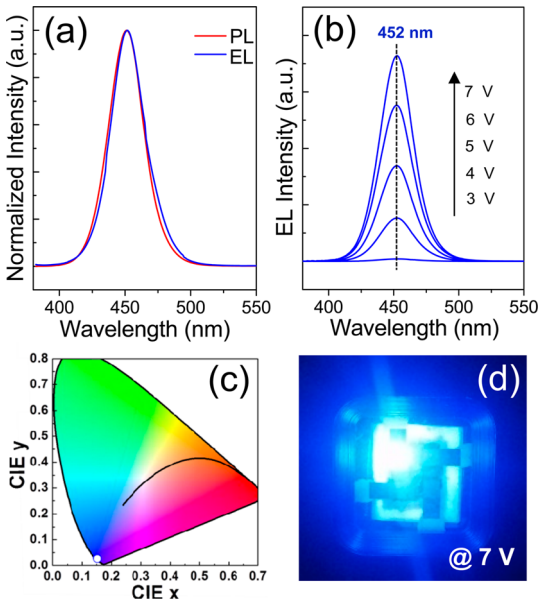

Figure 4. (a) Spectral comparison of PL of QD solution *versus* EL of QD-LED. (b) Evolution of EL spectra of QD-LED with increasing voltage. (c) CIE color coordinates of (0.153, 0.027) corresponding to the blue emission spectra in (b). (d) Electroluminescent image under an applied voltage of 7 V.

CONCLUSION

Synthesis of blue-emitting, OA-capped CdZnS/ZnS QDs, possessing a record high QY value of near-unity and a high PL stability against a repeated purification process, were demonstrated by adopting S-OA stock solution for ZnS shelling and extraordinarily long shelling duration up to 3 h. The resulting 3 h-shelled QDs exhibited a considerably large size of 11.5 nm with a thick shell of 2.6 nm, compared to those shelled for short periods of time. Using the QDs with different shelling durations of 0.5, 1, and 3 h, all-solution-processed, multilayered blue QD-LEDs were fabricated. The 3 h-shelled QD-LED showed the highest device performance of a maximum luminance of 2624 cd/m^2 at 7.5 V, maximum LE of 2.2 cd/A, and maximum EQE of

7.1% at 5 V. This excellent EQE was more than 4 times higher compared to the best blue QD-LED reported previously. The highest device efficiency from 3 h-shelled QD-based device was attributable to (i) an exceptional PL QY, (ii) a thick shell (leading to the suppression of nonradiative AR and inter-QD resonant energy transfer processes), and (iii) an alloyed core/shell interface with a smooth confinement potential (leading to the suppression of AR process) of 3 h-shelled QDs. Moreover, in the case of 3 h-shelled QD-LED, unusual spectral match of EL with PL and no change of EL spectra with increasing voltage were observed and discussed in conjunction with the presence of a thick shell.

EXPERIMENTAL SECTION

Synthesis of Blue-Emitting CdZnS/ZnS QDs. In a typical synthesis of CdZnS/ZnS QDs, 1 mmol of CdO and 10 mmol of Zn acetate were mixed with 7 mL of OA in 50 mL of 3-neck reactor. This mixture was heated to 150 °C with Ar purging. Then, 15 mL of ODE was added into the reactor at that temperature and the whole mixture was further heated. Upon reaching 310 °C, the first sulfur (S) stock solution of 1.6 mmol of S dissolved in 2.4 mL of ODE was swiftly injected into the above hot mixture, and the reaction was maintained at that temperature for 12 min for the growth of CdZnS core QDs. For the subsequent overcoating of ZnS shell, the second S stock solution of 4 mmol of S dissolved in 5 mL of OA was dropwisely introduced in a rate of ~0.5 mL/min, and the shelling reaction was maintained for 0.5−3 h. The resulting QDs were precipitated with the addition of an excess of ethanol and the following centrifugation (12 000 rpm, 10 min), and then purified three times by precipitation/dispersion method with a solvent combination of hexane/ethanol (10/40 in mL) using the same centrifugation condition, and the purified QDs were redispersed into hexane for the spin-deposition of EML.

Synthesis of ZnO NPs. ZnO NPs were synthesized based on the protocol reported in the literature as follows: 3 mmol of Zn acetate hydrate was dissolved in 30 mL of DMSO (dimethyl sulfoxide). Five millimoles of TMAH dissolved in 10 mL of ethanol was dropwisely added in a rate of ~8 mL/min to the above Zn solution, and the reaction proceeded at room temperature for 1 h. Then, ZnO NPs were precipitated by adding an excess of acetone and redispersed into ethanol for the spin-deposition of ETL.

Fabrication of Multilayered Blue QD-LEDs and Device Characterization. A patterned ITO glass substrate was cleaned sequentially with acetone and methanol, and then, finally UV-ozone treated for 20 min. First, a hole injection layer (HIL) of PEDOT:PSS (AI 4083) was spin-coated at 3000 rpm for 60 s, and then baked at 150 °C for 30 min in a N_2-fiiled glovebox. With th euse of a PVK solution of 0.05 g of PVK (average M_W = 25 000−50 000) dissolved in 5 mL of chlorobenzene, HTL was deposited on top of HIL with the same spinning baking conditions as above. With a QD dispersion in hexane with a concentration of ~25 mg/mL, EML of blue CdZnS/ZnS QDs was spin-deposited at 2000 rpm for 20 s and no baking followed. A transparent ethanol solution of ZnO NPs with a concentration of ~20 mg/mL was consecutively spin-coated at 1500 rpm for 60 s, followed by the baking at 60 °C for 30 min in the same glovebox. Finally, a 100 nm thick Al cathode was thermally evaporated on top of ETL, completing the multilayered structure of ITO/PEDOT:PSS/PVK/CdZnS/ZnS QDs/ZnO NPs/Al.

Characterization. Absorption and PL emission spectra were recorded with UV−visible absorption spectroscopy (Shimadzu, UV-2450) and a 500 W Xe lamp-equipped spectrophotometer (PSI Co. Ltd., Darsa Pro-5200), respectively. PL QYs of CdZnS/ZnS QDs were calculated by comparing their integrated emissions with that of a standard dye solution of 9,10-diphenylanthracene (QY of ~91%) in ethanol with an identical optical density of ~0.05 at 370 nm. TEM images of CdZnS core, CdZnS/ZnS core/shell QDs, and ZnO NPs were obtained using JEOL JEM-4010 electron microscope operated at an accelerating voltage of 400 kV. Field emission-SEM (Hitachi S-4300) operated at 10 kV was used to obtain information on the thicknesses of individual layers in multilayered QD-LED and the surface morphologies of the EML of QDs and the ETL of ZnO NPs. The chemical compositions of CdZnS/ZnS QDs were measured using an EDS (EDAX, Inc., Phoenix)-equipped SEM operated at 15 kV. EL spectra and luminance−current density−voltage characteristics of blue QD-LEDs were recorded with a Konica-Minolta CS-1000 spectroradiometer coupled with a Keithley 2400 voltage and current source under ambient conditions.

Conflict of Interest: The authors declare no competing financial interest.

Acknowledgment. This work was supported by the National Research Foundation of Korea (NRF) grant funded by the Korea government (MEST) (No. 2011-0013377 and 2012K001320), and also supported in part by Samsung Display Co., Ltd.

Supporting Information Available: PL emission spectra and chemical compositions of Zn/Cd ratio of CdZnS/ZnS QDs, TEM image of TOP-capped CdZnS/ZnS QDs and changes in PL QY of TOP-capped *versus* OA-capped CdZnS/ZnS QDs as a function of repetition number of purification, TEM images of CdZnS core QDs and ZnO nanoparticles, SEM images of ITO/PEDOT:PSS/PVK/QDs/ZnO NPs, luminous efficiency−luminance and power efficiency−voltage characteristics of blue emissive devices having the QDs with 0.5, 1, and 3 h shelling times, luminance−current density and luminous efficiency−external quantum efficiency as a function of driving voltage for TOP-capped CdZnS/ZnS QD-based LED, and voltage-dependent EL spectral red-shift and broadening of TOP-capped CdZnS/ZnS QD-based LED. This material is available free of charge *via* the Internet at http://pubs.acs.org.

REFERENCES AND NOTES

1. Colvin, V. L.; Schlamp, M. C.; Alivisatos, A. P. Light-Emitting Diodes Made from Cadmium Selenide Nanocrystals and a Semiconducting Polymer. *Nature* **1994**, *370*, 354–357.
2. Sun, Q.; Wang, Y. A.; Li, L. S.; Wang, D.; Zhu, T.; Xu, J.; Yang, C.; Li, Y. Bright, Multicoloured Light-Emitting Diodes Based on Quantum Dots. *Nat. Photonics* **2007**, *1*, 717–722.
3. Zhao, J.; Bardecker, J. A.; Munro, A. M.; Liu, M. S; Niu, Y.; Ding, I. K.; Luo, J.; Chen, B.; Jen, A. K. Y.; Ginger, D. S. Efficient CdSe/CdS Quantum Dot Light-Emitting Diodes Using a Thermally Polymerized Hole Transport Layer. *Nano Lett.* **2006**, *6*, 463–467.
4. Jang, E.; Jun, S.; Jang, H.; Lim, J.; Kim, B.; Kim, Y. White-Light-Emitting Diodes with Quantum Dot Color Converters for Display Backlights. *Adv. Mater.* **2010**, *22*, 3076–3080.
5. Jun, S.; Jang, E. Bright and Stable Alloy Core/Multishell Quantum Dots. *Angew. Chem., Int. Ed.* **2013**, *52*, 679–682.
6. Chen, Y.; Vela, J.; Htoon, H.; Casson, J. L.; Werder, D. J.; Bussian, D. A.; Klimov, V. I.; Hollingsworth, J. A. "Giant" Multishell CdSe Nanocrystal Quantum Dots with Suppressed Blinking. *J. Am. Chem. Soc.* **2008**, *130*, 5026–5027.
7. Anikeeva, P. O.; Halpert, J. E.; Bawendi, M. G.; Bulovic, V. Quantum Dot Light-Emitting Devices with Electroluminescence Tunable over the Entire Visible Spectrum. *Nano Lett.* **2009**, *9*, 2532–2536.
8. Bae, W. K.; Kwak, J.; Lim, J.; Lee, D.; Nam, M. K.; Char, K.; Lee, C.; Lee, S. Multicolored Light-Emitting Diodes Based on All-Quantum-Dot Multilayer Films Using Layer-by-Layer Assembly Method. *Nano Lett.* **2010**, *10*, 2368–2373.
9. Bae, W. K.; Kwak, J.; Park, J. W.; Char, K.; Lee, C.; Lee, S. Highly Efficient Green-Light-Emitting Diodes Based on

CdSe@ZnS Quantum Dots with a Chemical-Composition Gradient. *Adv. Mater.* **2009**, *21*, 1690–1694.
10. Bae, W. K.; Kwak, J.; Lim, J.; Lee, D.; Nam, M. K.; Char, K.; Lee, C.; Lee, S. Deep Blue Light-Emitting Diodes Based on $Cd_{1-x}Zn_xS$@ZnS Quantum Dots. *Nanotechnology* **2009**, *20*, 075202.
11. Ji, W.; Jing, P.; Fan, Y.; Zhao, J.; Wang, Y.; Kong, X. Cadmium-Free Quantum Dot Light Emitting Devices: Energy-Transfer Realizing Pure Blue Emission. *Opt. Lett.* **2013**, *38*, 7–9.
12. Stouwdam, J. W.; Janssen, R. A. J. Red, Green, and Blue Quantum Dot LEDs with Solution Processable ZnO Nanocrystal Electron Injection Layers. *J. Mater. Chem.* **2008**, *18*, 1889–1894.
13. Wood, V.; Panzer, M. J.; Halpert, J. E.; Caruge, J. M.; Bawendi, M. G.; Bulovic, V. Selection of Metal Oxide Charge Transport Layers for Colloidal Quantum Dot LEDs. *ACS Nano* **2009**, *3*, 3581–3586.
14. Qian, L.; Zheng, Y.; Xue, J.; Holloway, P. H. Stable and Efficient Quantum-Dot Light-Emitting Diodes Based on Solution-Processed Multilayer Structures. *Nat. Photonics* **2011**, *5*, 543–548.
15. Kwak, J.; Bae, W. K.; Lee, D.; Park, I.; Lim, J.; Park, M.; Cho, H.; Woo, H.; Yoon, D. Y.; Char, K.; *et al.* Bright and Efficient Full-Color Colloidal Quantum Dot Light-Emitting Diodes Using an Inverted Device Structure. *Nano Lett.* **2012**, *12*, 2362–2366.
16. Cho, K. S.; Lee, E. K.; Joo, W. J.; Jang, E.; Kim, T. H.; Lee, S. J.; Kwon, S. J.; Han, J. Y.; Kim, B. K.; Choi, B. L.; *et al.* High-Performance Crosslinked Colloidal Quantum-Dot Light-Emitting Diodes. *Nat. Photonics* **2009**, *3*, 341–345.
17. Kim, T. H.; Cho, K. S.; Lee, E. K.; Lee, S. J.; Chae, J.; Kim, J. W.; Kim, D. H.; Kwon, J. Y.; Amaratunga, G.; Lee, S. Y.; *et al.* Full-Colour Quantum Dot Displays Fabricated by Transfer Printing. *Nat. Photonics* **2011**, *5*, 176–182.
18. Tan, Z.; Zhang, F.; Zhu, T.; Xu, J.; Wang, A. Y.; Dixon, J. D.; Li, L.; Zhang, Q.; Mohney, S. E.; Ruzyllo, J. Bright and Color-Saturated Emission from Blue Light-Emitting Diodes Based on Solution-Processed Colloidal Nanocrystal Quantum Dots. *Nano Lett.* **2007**, *7*, 3803–3807.
19. Mashford, B. S.; Stevenson, M.; Popovic, Z.; Hamilton, C.; Zhou, Z.; Breen, C.; Steckel, J.; Bulovic, V.; Bawendi, M.; Coe-Sullivan, S.; *et al.* High-Efficiency Quantum-Dot Light-Emitting Devices with Enhanced Charge Injection. *Nat. Photonics* **2013**, *7*, 407–412.
20. Bae, W. K.; Nam, M. K.; Char, K.; Lee, S. Gram-Scale One-Pot Synthesis of Highly Luminescent Blue Emitting $Cd_{1-x}Zn_xS$/ZnS Nanocrystals. *Chem. Mater.* **2008**, *20*, 5307–5313.
21. Mahler, B.; Spinicelli, S.; Buil, S.; Quelin, X.; Hermier, J. P.; Dubertret, B. Towards Non-Blinking Colloidal Quantum Dots. *Nat. Mater.* **2008**, *7*, 659–664.
22. Garcia-Santamaria, F.; Chen, Y.; Vela, J.; Schaller, R. D.; Hollingsworth, J. A.; Klimov, V. I. Suppressed Auger Recombination in "Giant" Nanocrystals Boosts Optical Gain Performance. *Nano Lett.* **2009**, *9*, 3482–3488.
23. Htoon, H.; Malko, A. V.; Bussian, D.; Vela, J.; Chen, Y.; Hollingsworth, J. A.; Klimov, V. I. Highly Emissive Multiexcitons in Steady-State Photoluminescence of Individual "Giant" CdSe/CdS Core/Shell Nanocrystals. *Nano Lett.* **2010**, *10*, 2401–2407.
24. Ghosh, Y.; Mangum, B. D.; Casson, J. L.; Williams, D. J.; Htoon, H.; Hollingsworth, J. A. New Insights into the Complexities of Shell Growth and the Strong Influence of Particle Volume in Nonblinking "Giant" Core/Shell Nanocrystal Quantum Dots. *J. Am. Chem. Soc.* **2012**, *134*, 9634–9643.
25. Pal, B. N.; Ghosh, Y.; Brovelli, S.; Laocharoensuk, R.; Klimov, V. I.; Hollingsworth, J. A.; Htoon, H. 'Giant' CdSe/CdS Core/Shell Nanocrystal Quantum Dots as Efficient Electroluminescent Materials: Strong Influence of Shell Thickness on Light-Emitting Diode Performance. *Nano Lett.* **2012**, *12*, 331–336.
26. Wang, X.; Ren, X.; Kahen, K.; Hahn, M. A.; Rajeswaran, M.; Maccagnano-Zacher, S.; Silcox, J.; Cragg, G. E.; Efros, A. L.; Krauss, T. D. Non-Blinking Semiconductor Nanocrystals. *Nature* **2009**, *459*, 686–689.
27. Garcia-Santamaria, F.; Brovelli, S.; Viswanatha, R.; Hollingsworth, J. A.; Htoon, H.; Crooker, S. A.; Klimov, V. I. Breakdown of Volume Scaling in Auger Recombination in CdSe/CdS Heteronanocrystals: the Role of the Core-Shell Interface. *Nano Lett.* **2011**, *11*, 687–693.
28. Wood, V.; Panzer, M. J.; Caruge, J. M.; Halpert, J. E.; Bawendi, M. G.; Bulovic, V. Air-Stable Operation of Transparent, Colloidal Quantum Dot Based LEDs with a Unipolar Device Architecture. *Nano Lett.* **2010**, *10*, 24–29.
29. Wen, G. W.; Lin, J. Y.; Jiang, H. X.; Chen, Z. Quantum-Confined Stark Effects in Semiconductor Quantum Dots. *Phys. Rev. B* **1995**, *52*, 5913–5922.